Journal of Zhejiang University-SCIENCE A (Applied Physics & Engineering)
ISSN 1673-565X (Print); ISSN 1862-1775 (Online)
www.jzus.zju.edu.cn; link.springer.com
E-mail: jzus_a@zju.edu.cn

Modification of acidity in HZSM-5 zeolite for methane-methanol co-reaction[#*]

Bing-jie ZHOU[1], Zhi-xiang XI[1], Yue YU[1], Bin-bo JIANG[†‡1], Jing-dai WANG[1,2], Zu-wei LIAO[1], Zheng-liang HUANG[1], Yong-rong YANG[1,2]

[1]*Zhejiang Provincial Key Laboratory of Advanced Chemical Engineering Manufacture Technology, Department of Chemical and Biological Engineering, Zhejiang University, Hangzhou 310027, China*

[2]*State Key Laboratory of Chemical Engineering, Zhejiang University, Hangzhou 310027, China*

[†]E-mail: jiangbb@zju.edu.cn

Received Mar. 31, 2020; Revision accepted July 12, 2020; Crosschecked Jan. 14, 2021

Abstract: A co-reaction of methane with methanol over zeolite catalysts has emerged as a new approach to the long-standing challenge of methane transformation. However, the effect of catalyst acid properties on the co-reaction has been rarely studied. In this study, a series of HZSM-5 zeolites with comparable diffusion abilities and various acidities were synthesized directly through steaming with 100% water vapor at 693 K. The co-reaction of methane and methanol was subsequently evaluated. Brønsted acidity at 0.262 mmol/g was detected to reach the maximum methane conversion of 5.42% at 673 K, which was also the odd point in the relationship between acid concentration and C4 hydrogen transfer index. Moreover, the influence of methanol feed was investigated over parent and steamed ZSM-5 catalyst, with results showing that excessive acid sites or methanol molecules reduce methane conversion. It is proposed that acid sites adsorbed with methanol molecules construct the methane activation sites. Hence, a proper design of zeolite acidity should be achieved to obtain higher methane conversion in the co-reaction process.

Key words: Methane conversion; Methanol; Co-reaction; Acidity; HZSM-5
https://doi.org/10.1631/jzus.A2000126 **CLC number:** TQ032.4

1 Introduction

With high levels of CH_4 emission and the inevitable depletion of oil reserves, interest and demand are growing to find a direct method of converting methane to valuable products (Karakaya et al., 2016; Vollmer et al., 2018). Nevertheless, the high energy of the C–H bond at 435 kJ/mol makes it a huge challenge to make this conversion to upgraded petrochemicals (Xu et al., 2012; Cao et al., 2013; Spivey and Hutchings, 2014; Schwach et al., 2017). Traditional oxidative coupling reactions can convert methane to high value-added chemicals, but the large amount of CO and CO_2 produced reduces the carbon utilization efficiency greatly (He et al., 2019b). In current procedures, the conversion of pure methane in an anaerobic environment requires extreme temperature conditions (>973 K) under thermodynamic limitations (Morejudo et al., 2016).

Co-reaction, which creates more preferable converting conditions successfully, is one of the most efficient strategies to achieve methane conversion to olefins, alkanes, alcohols, etc. (Choudhary et al., 2005; Wang et al., 2016; Jarvis et al., 2018; Li et al., 2018; He et al., 2019a). For example, methane and propane could be converted to aromatics over an Mo-H-BEA

‡ Corresponding author
* Project supported by the National Natural Science Foundation of China (No. U1663222)
# Electronic supplementary materials: The online version of this article (https://doi.org/10.1631/jzus.A2000126) contains supplementary materials, which are available to authorized users
ORCID: Bin-bo JIANG, https://orcid.org/0000-0002-7072-1482

catalyst at 773 K through ^{13}C cross polarization/magic angle spinning (CP/MAS) nuclear magnetic resonance (NMR) spectrum (Luzgin et al., 2013). It has also been shown that methane and heptane could be transformed into hydrocarbons over a Zn-Ga/ZSM-5 catalyst at 673 K and 3 MPa (Li et al., 2018). It is worth noting that the co-reaction method reduces the activation barrier, and also activates methane at a lower temperature, improving carbon utilization.

Methanol is inexpensive and is readily produced from various sources; the reaction from methanol to hydrocarbons is exothermic, while the methane dehydro-aromatization process is endothermic. The co-reaction of methane with methanol is reported to overcome the inertness of C–H bonds in methane, while heat neutralization is also reached (Mier et al., 2010). The zeolite ZSM-5 has been widely used in this co-reaction due to its unique channel structure, thermal stability, acidity, and shape-selectivity (Mohammadparast et al., 2015). Over Mo/HZM-5, this co-reaction reaches a long time steady state (60 h) with high methane conversion rate (26.4%) and benzene-toluene-xylene (BTX) selectivity above 90% at 973 K (Liu et al., 2016). Through loading Ga, Zn, Mo, and In ions on ZSM-5 zeolites for methane conversion with methanol, it was proved that these ions activate methane in combination with zeolitic protons (Choudhary et al., 2005). Also, bimetallic supported ZSM-5 was found to lead to a maximum methane conversion of 15.5% with 88.7% aromatic selectivity at 923 K (Majhi and Pant, 2014).

Both metal cations and zeolite acidity are important for methane activation. Previous reports have mainly focused on the effect of the metal center on methane activation, such as the impact of metal content, metal species, and existing forms (Liu et al., 2016). In contrast, few studies have been conducted on the role of zeolite acidity in the methane-methanol co-reaction (Taifan and Baltrusaitis, 2016). Acidity can influence catalytic performance, lifetime, and coke formation in reaction processes (Gao et al., 2016). Studying the activation of methane by acidic sites of catalysts is important for guiding the design and synthesis of catalyst frameworks. Besides, it also lays the theoretical foundations of further research on the synergy between metal centers and acidic sites.

Research on the effect of acidity on catalytic performance has involved the preparation of a series of catalysts with different Si/Al ratios (Lin et al., 2014) or the destruction of the catalyst skeleton by means of post-treatments (steaming treatment, acid/alkali treatment) (Lin et al., 2015). The effects of Si/Al ratio on the performance of ZSM-5 in methanol aromatization were investigated in (Gao et al., 2016), but variation in crystallinity occurred, with considerable changes in specific surface area and pore volume. Though protonic acid properties strongly influence catalytic performance in zeolite catalytic reactions, studies have also shown that the impact of crystal size and pore properties on the catalytic performance of zeolites cannot be ignored (Fernandez et al., 2010; Mohammadparast et al., 2015; Niu et al., 2017).

Therefore, while maintaining the same crystal structure and pore diffusion properties of zeolites, the influence of acid properties on catalytic performance should clearly be studied. In the present study, the co-reaction of methane with methanol was studied over a series of steam-treated HZSM-5 zeolites. We primarily focused on the effects of zeolite acidity on methane conversion and product distributions. Based on our results, the correlation between acid concentration and methane conversion rate is discussed and the methane activation site is proposed.

2 Experimental

2.1 Catalyst preparation

Samples of HZSM-5 with a SiO_2/Al_2O_3 ratio of 25 were obtained from Nankai Catalyst Co., Ltd., China. Once catalyst powder was tableted under 30 kg pressure, tablets were crushed and sieved through 20–40 meshes (0.42–0.84 mm). Subsequently, it was calcined at 773 K in ambient air for 2 h to remove the residual template. The fresh catalyst (C-0) was loaded in the middle of a 10 mL tube reactor. Steaming was done in 100% water vapor at 0.6 $g_{H_2O}/g_{catalyst}/h$ and 693 K for 1.5 h, 3 h, 6 h, and 12 h. Catalysts were then dried at 378 K for 4 h. Catalysts in this series were named as C-1.5 (1.5 h treatment), C-3 (3 h treatment), C-6 (6 h treatment), and C-12 (12 h treatment), respectively.

2.2 Catalyst characterization

The X-ray diffraction (XRD) process was performed using an X'Pert PROX/PANalytical

diffractometer with a Cu-Kα X-ray source at 40 kV and 34 mA in the 2θ range 5°–80°, and a scan rate of 2 (°)/min. A scanning electron microscope (SEM; SU-8010) was used to collect SEM images. The element distribution over the zeolite surface was analyzed by energy dispersive X-ray (EDS; X-max80). The concentrations of Si and Al were recorded on an inductively coupled plasma-optical emission spectroscope (ICP-OES, Agilent 5110). A physical adsorption instrument (Micromeritics, ASAP2020) was used for N_2 adsorption experiments. The NH_3 temperature-programmed desorption (NH_3-TPD) was performed using a chemical adsorption instrument (Quantachrome, ASiQ). Data were collected with an ^{27}Al NMR spectra Bruker Avance III HD (400 MHz) nuclear magnetic resonance (NMR) spectrometer.

The intelligent gravimetric analyzer (IGA, Hiden analytical) was used to conduct the diffusion experiments. Catalyst samples were placed in the reactor and outgassed first in a vacuum environment at 673 K for a period of 24 h, at the end of which N_2 (300 mL/min) was introduced from the gas cylinder to flow through the catalysts for 3 h. During this process, the total mass of catalyst and nitrogen adsorbed in the pores was recorded. Fick's second law (Eq. (1)) was used to describe the diffusion of N_2 molecules in the pores of the zeolite catalyst and Eq. (2) was used to calculate the diffusion coefficient $D_{i,k}$.

$$\frac{\partial q_i}{\partial t} = D_{i,k}\left(\frac{\partial^2 q_i}{\partial r^2} + \frac{2}{r}\frac{\partial q_i}{\partial r}\right), \tag{1}$$

where q_i is the concentration of component i, t is the time, and r is the radius of the sample. The initial conditions are t=0, q_i=$q_{i,0}$. The boundary conditions are: r=0, $\frac{\partial q_i}{\partial r} = 0$; r=R_p, q_i=constant (where R_p is catalyst particle radius).

$$\frac{M_{i,t}}{M_{i,\infty}} = 1 - \sum_{n=1}^{\infty}\frac{6}{n^2\pi^2}\exp\left(\frac{-D_{i,k}n^2\pi^2 t}{R_p^2}\right), \tag{2}$$

where $M_{i,t}$ is the amount of component i adsorbed in the catalyst at time t, g; $M_{i,\infty}$ is the equilibrium adsorption amount of component i, g; $D_{i,k}$ is the configuration diffusion coefficient of component i in the catalyst, m^2/s.

2.3 Catalyst activity test

A sample of 0.96 g catalyst mixed with glass beads as an inert was loaded to the fixed-bed reactor at 673 K, 1 atm (1 atm=101 325 Pa). The co-reaction conditions were: $WHSV_{CH_3OH}$=2 h^{-1}, P_{CH_3OH}=30 kPa, P_{CH_4}=30 kPa (WHSV is the weight hourly space velocity, and P is the partial pressure). For comparative research, methanol feed experiments were carried out under the same catalyst and gas velocity with $WHSV_{CH_3OH}$=2 h^{-1} and P_{CH_3OH}=30 kPa. An online Agilent 7820A gas chromatograph (GC) was used to analyze product composition.

The conversion of methane and methanol, and the selectivity of products were calculated as follows:

$$\text{Conversion of } CH_4 = \frac{\omega(CH_4)_{inlet} - \omega(CH_4)_{outlet}}{\omega(CH_4)_{inlet}} \times 100\%, \tag{3}$$

$$\text{Conversion of } CH_3OH = \frac{\omega(CH_3OH)_{inlet} - \omega(CH_3OH)_{outlet}}{\omega(CH_3OH)_{inlet}} \times 100\%, \tag{4}$$

$$\text{Selectivity of product} = \omega(\text{product})_{outlet} / [\omega(CH_4)_{inlet} - \omega(CH_4)_{outlet} + \omega(CH_3OH)_{inlet} - \omega(CH_3OH)_{outlet}] \times 100\%, \tag{5}$$

where ω represents the CH_2-based mass fraction.

3 Results and discussion

3.1 Structural characterization of the zeolites

Fig. 1 shows the XRD patterns of fresh ZSM-5 and the zeolites of various acidities treated by steaming. Results indicate that all six zeolites exhibit MFI topology and high purity. The degree of the relative crystallinity, that was determined from the peak area between 2θ=22.5°–24.5° with a reference to C-0, is listed in Table 1. All treated samples show the same relative crystallinity after steam treatment.

The SEM images of zeolites are shown in Fig. 2, while Fig. 2a depicts the morphology of prismatic crystals, which is consistent with the description of the MFI phase described in (Bjørgen et al., 2008). A higher degree of aggregation in the crystal morphology is demonstrated in Figs. 2b–2e. After different steam treatments, the catalyst morphology remains the same.

Table 1 summarizes the results of elemental analysis of H-ZSM-5 samples by ICP-OES. The Si/Al ratio increases along with an increasing duration of steam treatment, as steaming leads to the extraction of Al from the framework with an impact on the Si/Al ratio (Groen et al., 2005).

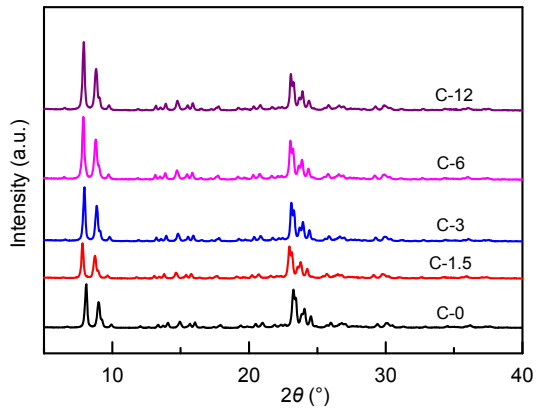

Fig. 1 XRD patterns of ZSM-5 samples

Table 1 Crystallinity and elemental analysis results for ZSM-5 samples

Catalyst	Relative crystallinity*	SiO_2/Al_2O_3** (molar ratio)
C-0	1.00	27.95
C-1.5	0.98	28.15
C-3	1.00	28.29
C-6	1.08	29.06
C-12	0.98	30.31

* By comparing the XRD peak intensities at 2θ of 22.5°–24.5° with those of the reference C-0 sample; ** Detected by ICP-OES

The element distributions of C-0 and C-12 are presented in Fig. 3, where the elements Si, O, and Al show uniform distributions on the surface of a single zeolite crystal. Points A and B were also selected for elemental scanning, with results shown in Table 2. Following 12 h of steam treatment, the Al content on the surface of the catalyst is reduced significantly, which is consistent with the results for ICP-OES.

Results for N_2 adsorption are shown in Fig. 4. Due to the presence of micropores, each sample shows a steep rise in the curves at a relative pressure of $10^{-6}<P/P_0<0.01$. At higher P/P_0 values, the adsorption curve displays a hysteresis loop and belongs to the type IV isotherm, while the closure point of the loop is at $P/P_0=0.45$, implying the presence of 1.7–2.0 nm mesopores. The Brunner-Emmet-Teller (BET) method and the *t*-plot method were applied to calculate the specific surface area and pore volume, while the density functional theory (DFT) method was used to calculate pore size distribution, with results shown in Table 3. Due to steaming, the area and volume of micopores decreased, and no significant differences were found among the steam-treated catalysts. The pore diameter of C-0 was 3.27 nm, while this increased to 3.74 nm after 12 h steaming as shown in Fig. 4b. It has been reported that steaming can generate mesopores by extracting Al from the zeolite lattice while reducing the number of micropores and increasing that of mesopores (Janssen et al., 2001), which is in accordance with our results.

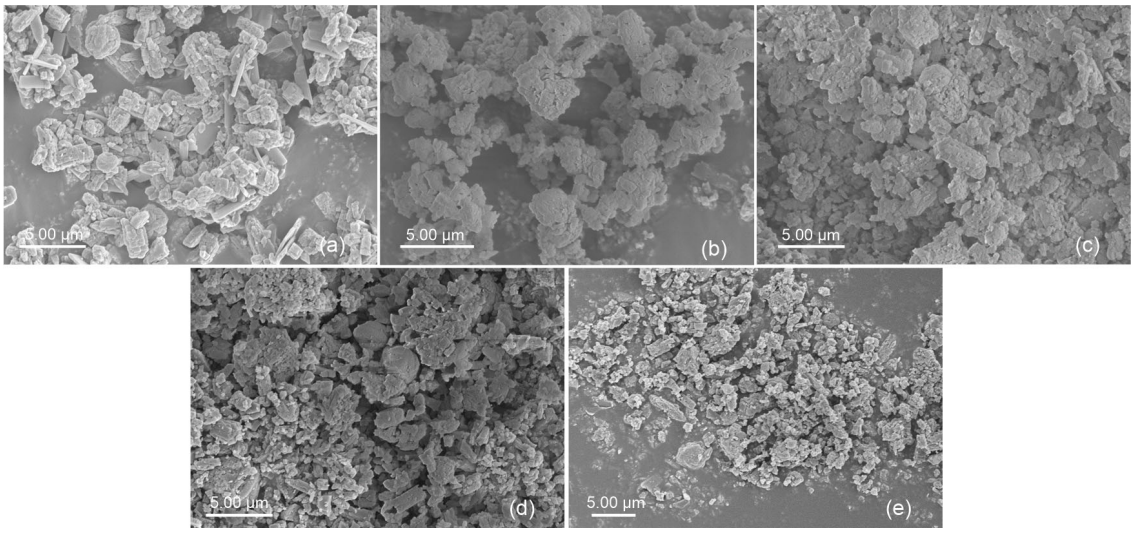

Fig. 2 SEM images of fresh ZSM-5 C-0 (a) and steam-treated ZSM-5 C-1.5 (b), C-3 (c), C-6 (d), and C-12 (e)

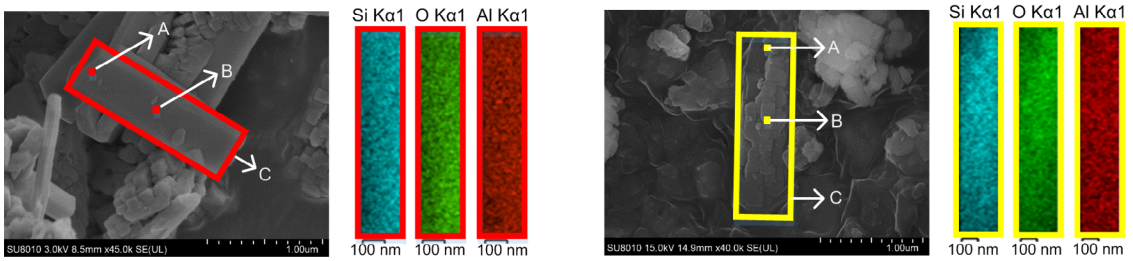

Fig. 3 EDS patterns of C-0 (a) and C-12 (b)

Table 2 Element contents of C-0 and C-12 tested by SEM-EDS (in weight)

Element	Element content (%)					
	C-0			C-12		
	Point A	Point B	Area C	Point A	Point B	Area C
O	65.47	67.96	67.75	70.10	69.18	69.01
Al	2.95	3.01	3.03	2.34	2.31	2.40
Si	31.58	29.03	29.21	27.56	28.51	28.59

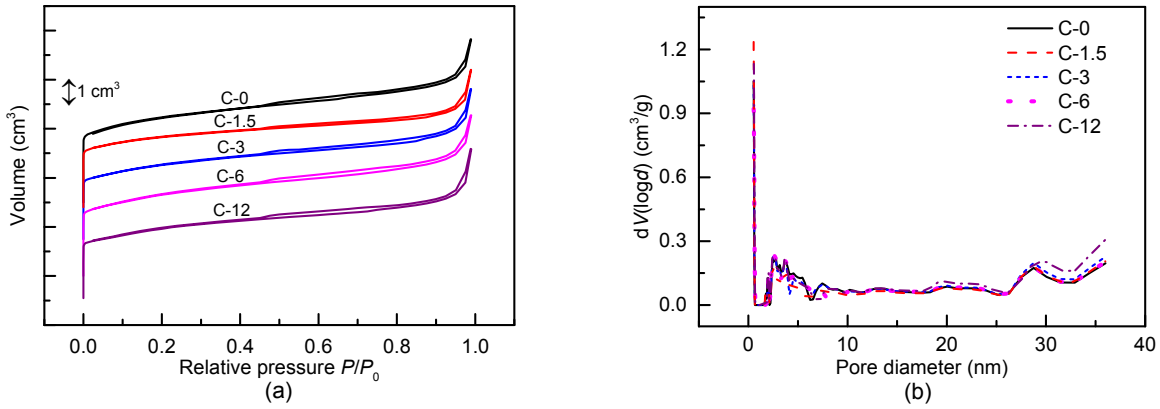

Fig. 4 N_2 adsorption results for the fresh and steam-treated ZSM-5 zeolites
V is the volume of adsorbed N_2; d is the diameter of pore in zeolite

Table 3 Textural properties of HZSM-5 and steam-treated catalysts

Catalyst	Surface area* (m^2/g)			Pore volume* (cm^3/g)			Pore diameter*	$D_{i,k}$**
	Total	Micro	External	Total	Micro	Meso	(nm)	($\times10^{-10}$ m^2/s)
C-0	418	308	110	0.34	0.13	0.21	3.27	1.04–4.18
C-1.5	387	281	106	0.32	0.12	0.20	3.32	1.39–5.54
C-3	389	274	115	0.34	0.12	0.22	3.48	0.77–3.10
C-6	381	270	111	0.33	0.12	0.21	3.43	0.91–3.66
C-12	386	274	112	0.36	0.12	0.24	3.74	0.71–2.84

* Detected by N_2 adsorption; ** Calculated through Eq. (2)

The diffusion coefficients of nitrogen in the zeolites at 673 K are listed in Table 3. The values of these coefficients are 0.77×10^{-10}–5.54×10^{-10} m^2/s, indicating that steaming has negligible effects on the diffusion behavior of small molecules.

3.2 Acidity of the zeolites

Results for NH_3-TPD are shown in Fig. 5, whereas Table 4 shows molar concentrations of acid in zeolites. As the duration of steam treatment

increases, acid concentration decreases from 1.166 to 0.474 mmol/g, and temperature (T) values for the peaks shift to the 'low' zone.

In order to confirm the distribution of aluminium within the ZSM-5 environment, ^{27}Al MAS NMR was performed on catalysts, with relevant spectra shown in Fig. 6. The strong signal at 54 ppm (1 ppm=1×10^{-6}) corresponds to tetrahedral framework aluminum (FAL) entering the zeolite framework, while the weak signal at 0 ppm corresponds to octahedral extra-framework aluminum (EFAL) atoms. The FAL and EFAL contents of the zeolites are calculated from the integrated peak intensities in the spectra and listed in Table 4. With steam treatment time increasing from 0 to 12 h, the mass fraction of EFAL increases from 11.28% to 21.85%, while the mass fraction of FAL decreases from 88.72% to 78.15% correspondingly. In fact, steaming has been shown to potentially cause the migration of framework aluminum, because bonds formed by Si-O-Al are generally less stable than those formed by Si-O-Si, and are susceptible to attack by water vapor (Brandenberger et al., 2011; Niwa et al., 2012). Thus, FAL atoms preferentially fall off the zeolite framework to form EFAL.

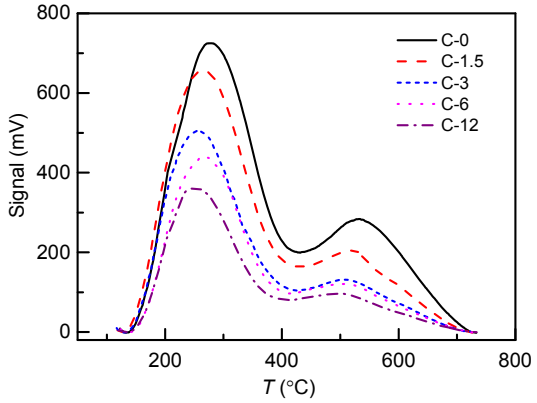

Fig. 5 NH_3-TPD profiles of fresh and steam-treated ZSM-5 zeolites

Table 4 Acid concentrations and Al distributions in fresh and steam-treated ZSM-5 zeolites

Sample	Acid concentration* (mmol/g)	Mass fraction (%)	
		EFAL**	FAL***
C-0	1.166	11.28	88.72
C-1.5	0.992	12.12	87.88
C-3	0.692	15.05	84.95
C-6	0.597	21.31	78.69
C-12	0.474	21.85	78.15

* Detected by NH_3-TPD; ** Calculated results of ^{27}Al NMR, $\delta_{Al}\approx$ 0 ppm; *** Calculated results of ^{27}Al NMR, $\delta_{Al}\approx$54 ppm (δ_{Al} is the chemical shift of ^{27}Al)

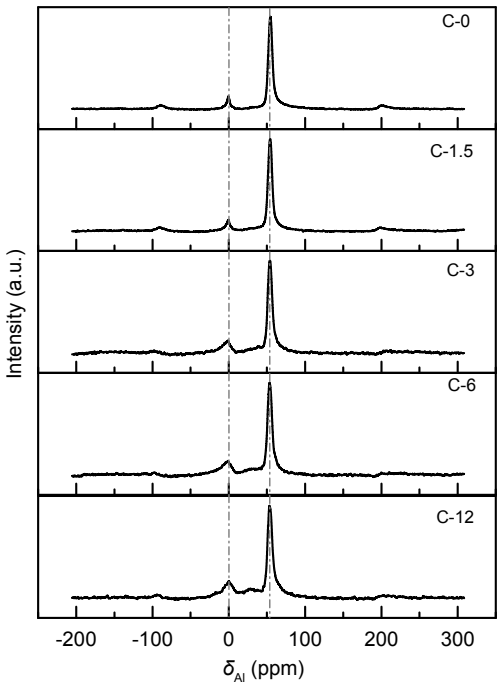

Fig. 6 ^{27}Al-MAS-NMR spectra of fresh and steam-treated ZSM-5 zeolites

3.3 Catalyst activity

3.3.1 Catalytic performance

The co-reaction of methane with methanol was carried out over C-0 and the steam-treated catalysts. At time of stream (TOS)=60 min, methanol conversion was 100% in all of the experiments. As shown in Fig. 7a, along with the increase of catalyst acid concentration, methane conversion increases initially before declining, reaching a maximum conversion of 5.42% at 0.692 mmol/g. Compared with the methane dehydro-aromatization reaction (Table S1), the co-reaction with methanol can activate methane at a lower temperature. The selectivity of alkanes and aromatics shows a continuous increment, while that of ethylene and propylene shows a reduction parallel with rising acid concentration.

For a comparison with the co-reaction, a catalytic reaction of methanol was conducted. The methanol was converted completely at TOS=60 min, with a product distribution shown in Fig. 7b. As acid concentration increases, the selectivity of alkanes and

aromatics grow in turn, while that of ethylene ($C_2^=$) and propylene ($C_3^=$) decreases. This could be attributed to a surge in the olefin cyclization reaction and the deep alkylation reaction parallel with the increase of acid concentration (Bjørgen et al., 2008; Ilias and Bhan, 2013; Gao et al., 2016).

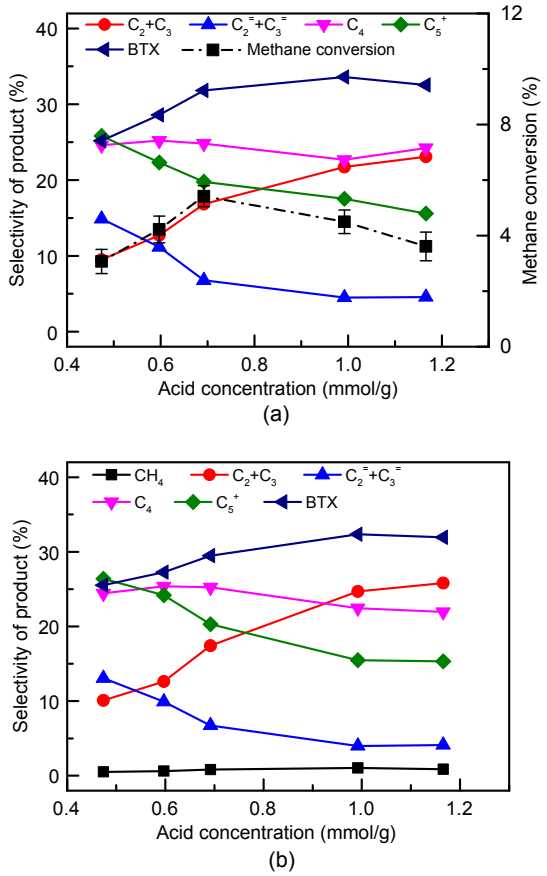

Fig. 7 Methane conversion and product distribution for the methane and methanol co-reaction (a) and the methanol reaction (b)

Methane-methanol co-reaction data: 0.96 g catalyst, T=673 K, $WHSV_{CH_3OH}$=2 h^{-1}, P_{CH_3OH}=30 kPa, P_{CH_4}=30 kPa, TOS=60 min; methanol reaction data: 0.96 g catalyst, T=673 K, $WHSV_{CH_3OH}$=2 h^{-1}, P_{CH_3OH}=30 kPa, TOS=60 min

When comparing Figs. 7a and 7b, products follow the same trend as acid concentration. This is attributed to the small amount of methane carbon converted, in comparison with methane (5%) and methanol (100%) conversion.

The C4 hydrogen transfer index (C4 HTI) is often used to describe the catalytic activity in the reaction from methanol to hydrocarbons (MTH) (Mentzel et al., 2009). This index is defined as the combined yields of isobutane and n-butane divided by the total yield of C4 alkanes and alkenes, and it constitutes a convenient measure of the hydrogen transfer activity of the catalyst (Bjørgen et al., 2008). As a function of acid concentration for methanol reaction and co-reaction of methane with methanol, it is presented in Fig. 8. With the acid concentration increasing from 0.474 mmol/g to 0.692 mmol/g, C4 HTI rises sharply from about 0.70 to 0.91; as acid concentration rises further from 0.692 mmol/g to 1.166 mmol/g, it rises more slowly from 0.91 to 0.94, as shown in Fig. 8. It is speculated that acids at 0.692 mmol/g are sufficient for the hydrogen transfer reaction under the current reaction conditions. Therefore, further increasing acid concentration would not show a significant effect on the C4 HTI index.

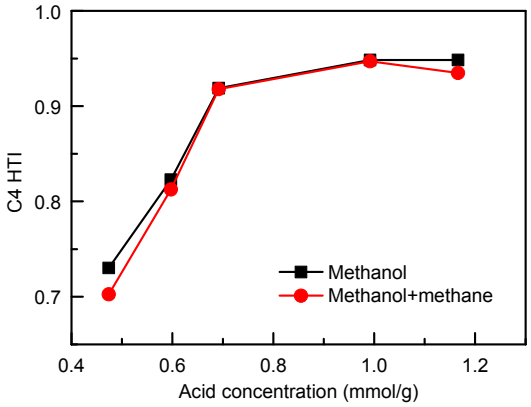

Fig. 8 C4 HTI index of the methanol reaction and the methane and methanol co-reaction

Methanol and methane co-reaction: 0.96 g catalyst, T=673 K, $WHSV_{CH_3OH}$=2 h^{-1}, P_{CH_3OH}=30 kPa, P_{CH_4}=30 kPa, TOS=60 min; methanol reaction: 0.96 g catalyst, T=673 K, $WHSV_{CH_3OH}$=2 h^{-1}, P_{CH_3OH}=30 kPa, TOS=60 min

3.3.2 Effect of methanol concentration on methane activation

The influence of methanol concentration on methane conversion was investigated over catalysts C-0 and C-3 under the following conditions: T=673 K, $WHSV_{CH_4}$=2 h^{-1}, P_{CH_4}=30 kPa, $WHSV_{CH_3OH}$=2 h^{-1}, 2.5 h^{-1}, and 3 h^{-1}. According to the results for catalyst C-0, methane conversion increases first with the increase of $WHSV_{CH_3OH}$, and then decreases after reaching a maximum at 2.5 h^{-1}, as shown in Fig. 9a. On the C-3 catalyst (Fig. 9b), methane conversion

gradually decreases as $WHSV_{CH_3OH}$ increases, with a maximum at 2 h^{-1}.

Based on the conclusion in Section 3.3.1, acid concentration is sufficient for the co-reaction under a current feed condition of WHSV=2 h^{-1}. By further increasing WHSV, acid sites would gradually reach adsorption saturation, and excess methanol molecules would compete with methane molecules in the system resulting in a decrease in methane conversion. As acid concentration in C-3 is lower than that in C-0, as space velocity increases, C-3 reaches the maximum methanol conversion first at 2 h^{-1}, while C-0 reaches this point later at 2.5 h^{-1}.

3.3.3 Proposal of methane activation sites in the co-reaction

Active sites for methane conversion do not exist on zeolites at 673 K (Taifan and Baltrusaitis, 2016), but can form when methanol is present. In co-reaction conditions, methanol is the first molecule to be adsorbed at active acid sites, which can be readily understood from the 126 kJ/mol difference between the proton affinities of methane (628 kJ/mol) and methanol (754 kJ/mol) (Sowerby et al., 1996; Haw, 2002; Chang et al., 2007). In the ZSM-5 catalyst, Brønsted acids are associated with four-coordinated FAL, while Lewis acid sites correspond to EFAL (Yu et al., 2011). The catalytic activity with aluminum oxide was also observed (Table S2). Aluminum oxide is not active in the conversion of methane and methanol, which means that Brønsted acids are the only effective active centers for the co-reaction (Sharanda et al., 1995; Li et al., 2011).

As is shown in Fig. 7, methane conversion reaches its maximum on catalyst C-3, which contains Brønsted acids at 0.262 mmol/g (Fig. S1). Methanol-adsorbed Brønsted acid sites form the active centers for methane activation. However, methanol is more easily adsorbed compared with methane. Therefore, excess methanol in the system compete with methane and is not conducive to methane conversion, which is consistent with results shown in Fig. 9.

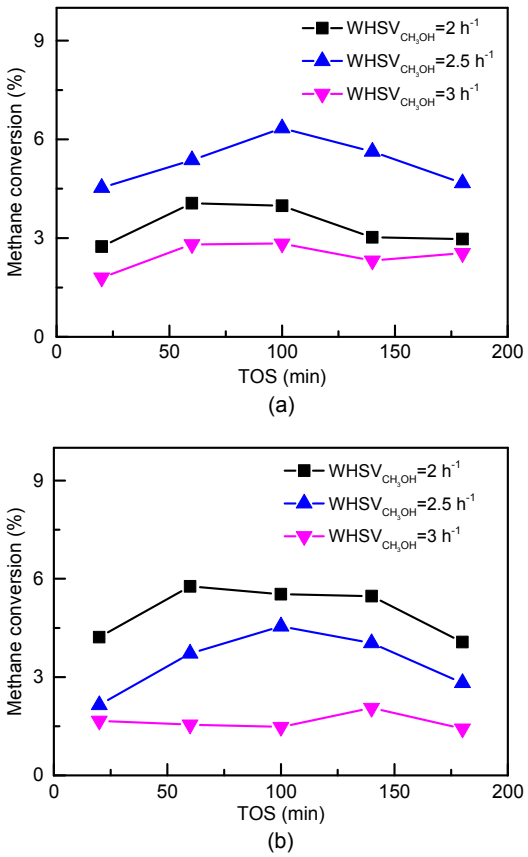

Fig. 9 Methane conversion in the methane and methanol co-reaction on catalyst C-0 (a) and catalyst C-3 (b)
Reaction conditions: T=673 K, P_{CH_3OH}=0.1 MPa, P_{CH_4}=30 kPa, $WHSV_{CH_4}$=2 h^{-1}, $WHSV_{CH_3OH}$=2 h^{-1}, 2.5 h^{-1}, and 3 h^{-1}

4 Conclusions

In this study, HZSM-5 zeolites with different acid concentrations were synthesized through steam treatment, and were used for co-reaction of methane with methanol at 673 K, 1 atm.

With an increasing duration of treatment, the acid concentration of the catalyst declines significantly regardless of crystal size, pore structure, or diffusion properties, which are similar or comparable among catalysts.

As the acid concentration in zeolite increases, methane conversion reaches a maximum of 5.42% on zeolite C-3, which contains Brønsted acids at 0.262 mmol/g. Furthermore, the effect of methanol concentration on methane conversion differs on fresh and steam-treated catalysts, while the maximum methane conversion rate is reached at $WHSV_{CH_3OH}$= 2.5 h^{-1} on C-0 and at $WHSV_{CH_3OH}$=2 h^{-1} on C-3.

On the basis of these results, it is proposed that methane is activated at acid sites of the zeolite that has methanol molecules adsorbed. Excessive amounts of

catalyst acid or too many methanol molecules inhibit methane activation. This provides guidance for catalyst selection in the co-reaction of methane with methanol, aimed to achieve higher methane conversion rates under mild conditions.

Contributors

Bin-bo JIANG and Bing-jie ZHOU designed the research. Bing-jie ZHOU and Zhi-xiang XI processed the corresponding data. Bing-jie ZHOU wrote the first draft of the manuscript. Yue YU and Jing-dai WANG helped to organize the manuscript. Zu-wei LIAO, Zheng-liang HUANG, and Yong-rong YANG revised and edited the final version.

Conflict of interest

Bing-jie ZHOU, Zhi-xiang XI, Yue YU, Bin-bo JIANG, Jing-dai WANG, Zu-wei LIAO, Zheng-liang HUANG, and Yong-rong YANG declare that they have no conflict of interest.

Reference

Bjørgen M, Joensen F, Spangsberg Holm M, et al., 2008. Methanol to gasoline over zeolite H-ZSM-5: improved catalyst performance by treatment with NaOH. *Applied Catalysis A: General*, 345(1):43-50. https://doi.org/10.1016/j.apcata.2008.04.020

Brandenberger S, Kröcher O, Casapu M, et al., 2011. Hydrothermal deactivation of Fe-ZSM-5 catalysts for the selective catalytic reduction of NO with NH_3. *Applied Catalysis B: Environmental*, 101(3-4):649-659. https://doi.org/10.1016/j.apcatb.2010.11.006

Cao ZW, Jiang HQ, Luo HX, et al., 2013. Natural gas to fuels and chemicals: improved methane aromatization in an oxygen-permeable membrane reactor. *Angewandte Chemie International Edition*, 52(51):13794-13797. https://doi.org/10.1002/anie.201307935

Chang FX, Wei YX, Liu XB, et al., 2007. A mechanistic investigation of the coupled reaction of *n*-hexane and methanol over HZSM-5. *Applied Catalysis A: General*, 328(2):163-173. https://doi.org/10.1016/j.apcata.2007.06.005

Choudhary VR, Mondal KC, Mulla SA, 2005. Simultaneous conversion of methane and methanol into gasoline over bifunctional Ga-, Zn-, In-, and/or Mo-modified ZSM-5 zeolites. *Angewandte Chemie International Edition*, 44(28):4381-4385. https://doi.org/10.1002/anie.200500694

Fernandez C, Stan I, Gilson JP, et al., 2010. Hierarchical ZSM-5 zeolites in shape-selective xylene isomerization: role of mesoporosity and acid site speciation. *Chemistry–A European Journal*, 16(21):6224-6233. https://doi.org/10.1002/chem.200903426

Gao Y, Zheng BH, Wu G, et al., 2016. Effect of the Si/Al ratio on the performance of hierarchical ZSM-5 zeolites for methanol aromatization. *RSC Advances*, 6(87):83581-83588. https://doi.org/10.1039/c6ra17084f

Groen JC, Moulijn JA, Pérez-Ramírez J, 2005. Decoupling mesoporosity formation and acidity modification in ZSM-5 zeolites by sequential desilication-dealumination. *Microporous and Mesoporous Materials*, 87(2):153-161. https://doi.org/10.1016/j.micromeso.2005.07.050

Haw JF, 2002. Zeolite acid strength and reaction mechanisms in catalysis. *Physical Chemistry Chemical Physics*, 4(22):5431-5441. https://doi.org/10.1039/b206483a

He P, Jarvis JS, Meng SJ, et al., 2019a. Co-aromatization of methane with propane over Zn/HZSM-5: the methane reaction pathway and the effect of Zn distribution. *Applied Catalysis B: Environmental*, 250:99-111. https://doi.org/10.1016/j.apcatb.2019.03.011

He P, Wang AG, Meng SJ, et al., 2019b. Impact of Al sites on the methane co-aromatization with alkanes over Zn/HZSM-5. *Catalysis Today*, 323:94-104. https://doi.org/10.1016/j.cattod.2018.05.051

Ilias S, Bhan A, 2013. Mechanism of the catalytic conversion of methanol to hydrocarbons. *ACS Catalysis*, 3(1):18-31. https://doi.org/10.1021/cs3006583

Janssen AH, Koster AJ, de Jong KP, 2001. Three-dimensional transmission electron microscopic observations of mesopores in dealuminated zeolite Y. *Angewandte Chemie International Edition*, 40(6):1102-1104. https://doi.org/10.1002/1521-3773(20010316)40:6<1102::aid-anie11020>3.0.co;2-6

Jarvis J, Wong A, He P, et al., 2018. Catalytic aromatization of naphtha under methane environment: effect of surface acidity and metal modification of HZSM-5. *Fuel*, 223:211-221. https://doi.org/10.1016/j.fuel.2018.03.045

Karakaya C, Morejudo SH, Zhu HY, et al., 2016. Catalytic chemistry for methane dehydroaromatization (MDA) on a bifunctional Mo/HZSM-5 catalyst in a packed bed. *Industrial & Engineering Chemistry Research*, 55(37):9895-9906. https://doi.org/10.1021/acs.iecr.6b02701

Li L, Stroobants C, Lin KF, et al., 2011. Selective conversion of trioses to lactates over Lewis acid heterogeneous catalysts. *Green Chemistry*, 13(5):1175-1181. https://doi.org/10.1039/c0gc00923g

Li QY, He P, Jarvis J, et al., 2018. Catalytic co-aromatization of methane and heptane as an alkane model compound over Zn-Ga/ZSM-5: a mechanistic study. *Applied Catalysis B: Environmental*, 236:13-24. https://doi.org/10.1016/j.apcatb.2018.05.006

Lin LF, Qiu CF, Zhuo ZX, et al., 2014. Acid strength controlled reaction pathways for the catalytic cracking of 1-butene to propene over ZSM-5. *Journal of Catalysis*, 309:136-145. https://doi.org/10.1016/j.jcat.2013.09.011

Lin LF, Zhao SF, Zhang DW, et al., 2015. Acid strength controlled reaction pathways for the catalytic cracking of

1-pentene to propene over ZSM-5. *ACS Catalysis*, 5(7): 4048-4059. https://doi.org/10.1021/cs501967r

Liu Y, Li DF, Wang TY, et al., 2016. Efficient conversion of methane to aromatics by coupling methylation reaction. *ACS Catalysis*, 6(8):5366-5370. https://doi.org/10.1021/acscatal.6b01362

Luzgin MV, Toktarev AV, Parmon VN, et al., 2013. Coaromatization of methane with propane on Mo-containing zeolite H-BEA: a solid-state NMR and GC-MS study. *The Journal of Physical Chemistry C*, 117(44):22867-22873. https://doi.org/10.1021/jp4071357

Majhi S, Pant KK, 2014. Direct conversion of methane with methanol toward higher hydrocarbon over Ga modified Mo/H-ZSM-5 catalyst. *Journal of Industrial and Engineering Chemistry*, 20(4):2364-2369. https://doi.org/10.1016/j.jiec.2013.10.014

Mentzel UV, Shunmugavel S, Hruby SL, et al., 2009. High yield of liquid range olefins obtained by converting *i*-propanol over zeolite H-ZSM-5. *Journal of the American Chemical Society*, 131(46):17009-17013. https://doi.org/10.1021/ja907692t

Mier D, Aguayo AT, Gayubo AG, et al., 2010. Synergies in the production of olefins by combined cracking of n-butane and methanol on a HZSM-5 zeolite catalyst. *Chemical Engineering Journal*, 160(2):760-769. https://doi.org/10.1016/j.cej.2010.04.016

Mohammadparast F, Halladj R, Askari S, 2015. The crystal size effect of nano-sized ZSM-5 in the catalytic performance of petrochemical processes: a review. *Chemical Engineering Communications*, 202(4):542-556. https://doi.org/10.1080/00986445.2014.952815

Morejudo SH, Zanón R, Escolástico S, et al., 2016. Direct conversion of methane to aromatics in a catalytic co-ionic membrane reactor. *Science*, 353(6299):563-566. https://doi.org/10.1126/science.aag0274

Niu XJ, Gao J, Wang K, et al., 2017. Influence of crystal size on the catalytic performance of H-ZSM-5 and Zn/H-ZSM-5 in the conversion of methanol to aromatics. *Fuel Processing Technology*, 157:99-107. https://doi.org/10.1016/j.fuproc.2016.12.006

Niwa M, Sota S, Katada N, 2012. Strong Brønsted acid site in HZSM-5 created by mild steaming. *Catalysis Today*, 185(1):17-24. https://doi.org/10.1016/j.cattod.2011.09.028

Schwach P, Pan XL, Bao XH, 2017. Direct conversion of methane to value-added chemicals over heterogeneous catalysts: challenges and prospects. *Chemical Reviews*, 117(13):8497-8520. https://doi.org/10.1021/acs.chemrev.6b00715

Sharanda LF, Shimansky AP, Kulik TV, et al., 1995. Study of acid-base surface properties of pyrogenic γ-aluminium oxide. *Colloids and Surfaces A: Physicochemical and Engineering Aspects*, 105(2-3):167-172. https://doi.org/10.1016/0927-7757(95)03265-7

Sowerby B, Becker SJ, Belcher LJ, 1996. Modeling of 2-methylpentane cracking: the application of adsorption equilibrium constants estimated using proton affinities. *Journal of Catalysis*, 161(1):377-386. https://doi.org/10.1006/jcat.1996.0195

Spivey JJ, Hutchings G, 2014. Catalytic aromatization of methane. *Chemical Society Reviews*, 43(3):792-803. https://doi.org/10.1039/c3cs60259a

Taifan W, Baltrusaitis J, 2016. CH_4 conversion to value added products: potential, limitations and extensions of a single step heterogeneous catalysis. *Applied Catalysis B: Environmental*, 198:525-547. https://doi.org/10.1016/j.apcatb.2016.05.081

Vollmer I, Li GN, Yarulina I, et al., 2018. Relevance of the Mo-precursor state in H-ZSM-5 for methane dehydroaromatization. *Catalysis Science & Technology*, 8(3): 916-922. https://doi.org/10.1039/c7cy01789h

Wang AG, He P, Yung M, et al., 2016. Catalytic co-aromatization of ethanol and methane. *Applied Catalysis B: Environmental*, 198:480-492. https://doi.org/10.1016/j.apcatb.2016.06.013

Xu J, Zheng AM, Wang XM, et al., 2012. Room temperature activation of methane over Zn modified H-ZSM-5 zeolites: insight from solid-state NMR and theoretical calculations. *Chemical Science*, 3(10):2932-2940. https://doi.org/10.1039/c2sc20434g

Yu ZW, Li SH, Wang Q, et al., 2011. Brønsted/Lewis acid synergy in H-ZSM-5 and H-MOR zeolites studied by ^{1}H and ^{27}Al DQ-MAS solid-state NMR spectroscopy. *The Journal of Physical Chemistry C*, 115(45):22320-22327. https://doi.org/10.1021/jp203923z

List of electronic supplementary materials

Table S1 Comparison of methane dehydro-aromatization reactions and co-reaction of methane and methanol

Table S2 Catalytic performance of methane and methanol co-reaction

Fig. S1 Infrared spectra of catalyst C-3